PERGAMON

International Journal of Heat and Mass Transfer 42 (1999) 1775–1790

International Journal of HEAT and MASS TRANSFER

Vaporization, melting and heat conduction in the laser drilling process

Yuwen Zhang, A. Faghri*

Department of Mechanical Engineering, University of Connecticut, Storrs, CT 06269-3139, U.S.A.

Received 19 June 1998; in final form 10 August 1998

Abstract

Melting and vaporization phenomena during the laser drilling process are investigated in this paper. The locations of the solid–liquid and liquid–vapor interfaces were obtained by solving energy conservation equations at the interfaces. The dependence of saturation temperature on the back pressure is taken into account by using the Clausius/Clapeyron equation. The conduction heat loss to the solid is also included in the model and is solved by using an integral approximate method. The results show that the fraction of the heat lost through conduction to the solid is very small and its effect on the vaporization process is not significant. On the other hand, the conduction heat loss significantly reduces the thickness of the liquid layer, which becomes the recast layer after drilling.

Nomenclature

a dimensionless curvature parameter of solid–liquid interface
c_p specific heat [J kg^{-1} K^{-1}]
dA dimensionless infinitesimal cross section area
F fraction of heat
f functions in equations (2a) and (3a)
h_{lv} latent heat of vaporization [J kg^{-1}]
H_{lv} dimensionless latent heat of vaporization $= h_{lv}/(R_g T_{sat,0})$
h'_{lv} revised latent heat of vaporization $= h_{lv} + c_{pl}(T_{sat} - T_m)/2$ [J kg^{-1}]
h_{sl} latent heat of melting [J kg^{-1}]
I laser intensity [W m^{-2}]
I_0 laser intensity at the center of the beam [W m^{-2}]
k thermal conductivity [W m^{-1} K^{-1}]
MR material removal rate [mg s^{-1}]
n coordinate along normal direction of the interface
N grid number in radial direction
N_i dimensionless laser intensity of laser beam $= c_{pl} R \alpha_{abs} I_0/k_l h_{lv}$
N_{p0} dimensionless ambient pressure $= \gamma p_0 c_{pl} R/[(\gamma+1)k_l\sqrt{\gamma R_g T_{sat,0}}]$
N_α thermal diffusivity ratio $= \alpha_s/\alpha_l$
p_0 ambient pressure [Pa]
P_{max} peak power of the laser beam [W]
r radial coordinate [m]
R radius of the laser beam (at $1/e$) [m]
R_g gas constant of the metal vapor [J kg^{-1} K^{-1}]
R_h latent heat ratio $= h_{lv}/h_{sl}$
s location of interface [m]
S dimensionless location of interface $= s/R$
Sc subcooling parameter $= c_{ps}(T_m - T_i)/h_{sl}$
Ste Stefan number $= c_{pl}(T_{sat} - T_m)/h_{lv}$
t time [s]
t_p pulse-on time [s]
T temperature [K]
V_n dimensionless solid–liquid interface velocity along n-direction
z axial coordinate [m]
Z dimensionless axial coordinate $= z/R$.

Greek symbols
α thermal diffusivity [m^2 s^{-1}]
α_{abs} absorptivity
γ ratio of specific heats of metal gas
δ dimensionless thermal penetration depth in the solid
$\Delta\eta$ grid size
$\Delta\tau$ dimensionless time step
η dimensionless radial coordinate $= r/R$

* Corresponding author. Tel.: 001 860 486 2221; fax: 001 860 486 0318; e-mail: faghri@eng2.uconn.edu

0017–9310/98/$ - see front matter
PII: S0017–9310(98)000268–3

θ_{l0} dimensionless surface temperature at the liquid surface $=(T_{l0}-T_m)/(T_{sat,0}-T_m)$
θ_m ratio of melting point and saturation temperature at the ambient pressure $=T_m/T_{sat,0}$
θ_s dimensionless temperature in the solid $=(T_s-T_i)/(T_m-T_i)$
ρ density [kg m^{-3}]
τ dimensionless time $=\alpha_l t/R^2$
τ_p dimensionless pulse-on time.

Subscripts
cr critical value
e vaporization
i initial
l liquid
m melting
s solid
sat saturation
sat,0 saturation value at ambient pressure
1 liquid–vapor interface
2 solid–liquid interface.

1. Introduction

The laser drilling process is very important in many industries which include automotive, aerospace, electronics and materials processing. It is a very complex process since both melting and vaporization are accomplished. Considerable research has been carried out to develop a theoretical laser drilling model and many detailed investigations are in the existing literature. A detailed review including various assumptions and simplifications are discussed by Ganesh et al. [1]. Paek and Gagliano [2] proposed a theoretical solution to predict the temperature profile and tangential stress distribution of the laser drilling process. Von Allmen [3] analyzed the drilling velocity and drilling efficiency by using a 1-D transient gas dynamic model. Chan and Mazumder [4] proposed a 1-D steady state model to predict the damage done by vaporization and liquid expulsion due to laser-material interaction. Both phase change heat transfer and gas dynamics were taken into account in their study. The limitation of the above works is that the laser drilling process was modeled as a 1-D problem but actual laser drilling processes are obviously transient 2-D or 3-D problems.

In order to overcome the drawbacks of the early research works, Armon et al. [5] formulated a 2-D metal drilling problem based on the enthalpy balance method and solved the problem by using the Crank–Nicholson method. They also conducted experimental investigations on metal drilling with a CO_2 laser beam [6] and analyzed the experimental results by using their theoretical model in ref. [5]. Kar and Mazumder [7] proposed a 2-D transient model to predict the shape of laser drilled holes by solving the energy conservation equation (Stefan condition) at various points along the liquid–solid and liquid–vapor interfaces. However, the shape of the laser drilled hole was simply assumed to be a combination of a parabola at the bottom and straight line at the sides. Kar et al. [8] improved the physical model of ref. [7] by considering the effect of assist gas and multiple reflection inside the cavity. However, the assumption of hole geometry used by Kar and Mazumder [7] was not removed by Kar et al. [8].

The loss of energy due to conduction to the workpiece on the laser drilling was not taken into account in Kar and Mazumder [7], Kar et al. [8]. The effect of conduction heat loss to the workpiece in laser cutting process have been investigated by Modest and Abakians [9] and Modest [10]. They concluded that the effect of conduction heat loss is significant for the case of CW laser cutting and is insignificant for case of pulse laser cutting. However, the change of phase of the medium from solid to vapor was assumed to occur in one step at a single vaporization temperature, which was not true if metal workpiece was cut by laser. Gordon et al. [11] studied the laser drilling on a diamond film numerically and their result indicate a strong preference for pulsed laser operation over CW laser because higher thermal efficiencies are attained. Ganesh et al. [1, 12] also developed a very detailed numerical model and complete physical model for the laser drilling process by employing a free surface and phase change simulation. The computer time was relatively large since it took 91 h on a SUN SPARC station to generate 281 μs of real time laser drilling data.

Analytical model of laser machining process by considering the heat transfer in the melt and solid simultaneously were not found in the existing literature. In order to provide a simple and reliable model to predict the geometric shape of the laser drilled hole, a new model describing the laser drilling process will be developed. The restrictions of the hole geometry used in refs [7, 8] will be removed. The dependence of saturation temperature on the back pressure will also be taken into account. The conduction heat loss to the workpiece will also be included in the model. The thermal modeling of laser drilling process with the effect of conduction heat loss to the workpiece requires appropriate modeling and solution of a non-linear conduction problem with two moving boundaries: liquid–vapor and solid–liquid interfaces. In this paper, melting and vaporization, conjugated with conduction in the workpiece, will be solved analytically. The effect of various parameters on the laser drilling process will also be discussed.

2. Interfacial energy balances

Figure 1 shows the physical model of the laser drilling process. A laser beam with a intensity of $I(r, t)$ is pro-

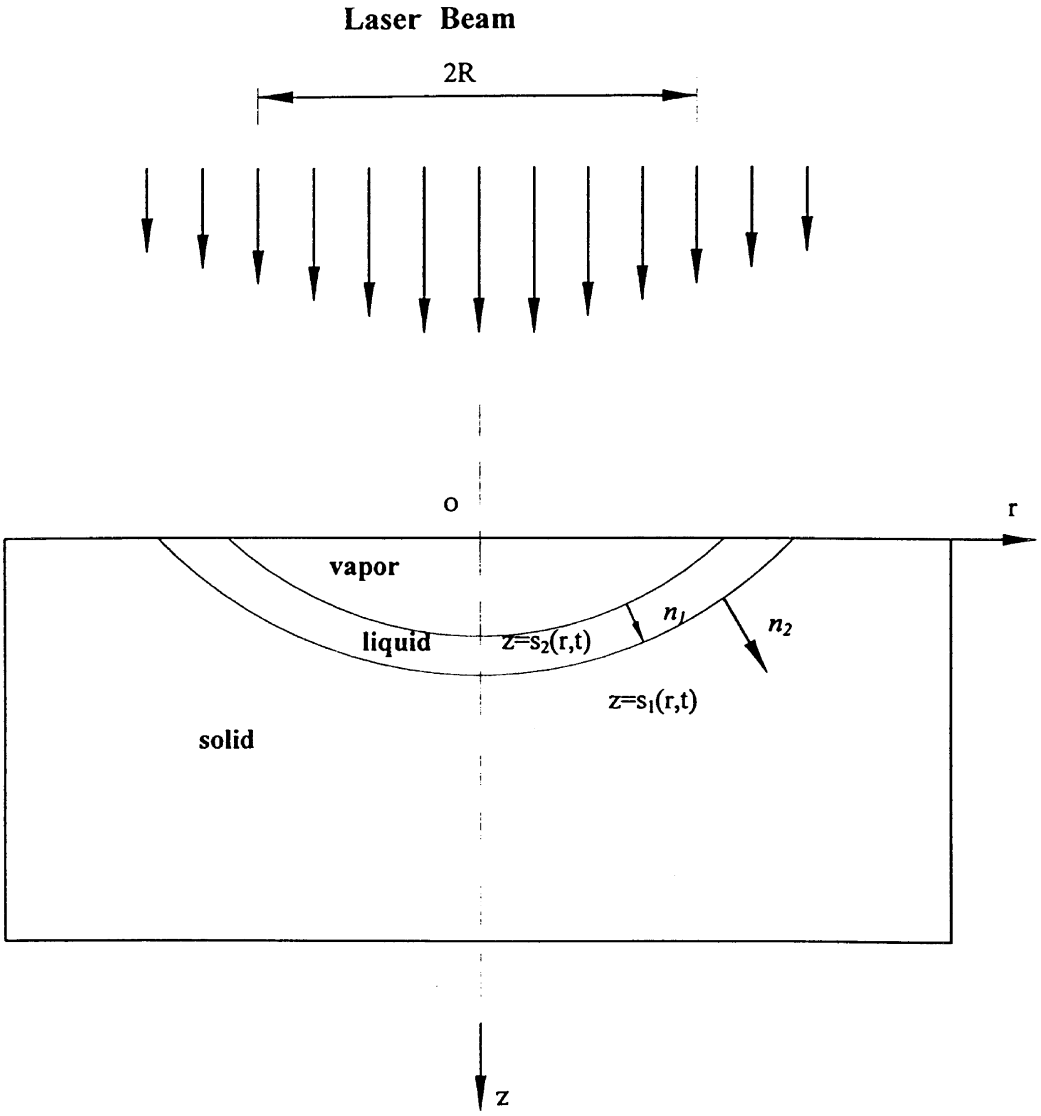

Fig. 1. Physical model of laser drilling process.

duced and directed towards a solid target material at an initial temperature of $T_i < T_m$, which absorbs a fraction of the incident light energy. The laser beam produces a very intensive heat flux to the solid which brings the temperature of solid to its melting point and then melts the solid and vaporizes the resulting liquid. The following assumptions will be needed in order to analyze the laser drilling process:

(1) The target material is opaque, i.e., the incident laser energy is instantly converted into heat at the surface of the target material and the laser beam does not penetrate into the target materials. This assumption is valid for good conductor of electricity, such as metal, because the damping of laser energy occurred in a very shallow penetrate depth.
(2) No plasma is generated in the laser drilled hole. This assumption is somewhat questionable for metals target materials. However, the effect of plasma can be ignored if pulse-on time is much shorter than the pulse-off time because the plasma can be extinguished between pulses [8].
(3) Liquid metal flow inside the hole is neglected and the temperature distribution in the liquid metal is assumed to be linear [8]. The sensible heat that is required to bring the liquid layer temperature to the average value of saturation temperature and melting point is added to the latent heat of vaporization to

account for the unsteady state effect, i.e.

$$h'_{\mathrm{lv}} = h_{\mathrm{lv}} + \tfrac{1}{2} c_{\mathrm{pl}}(T_{\mathrm{sat}} - T_{\mathrm{m}}). \quad (1)$$

(4) The liquid and solid properties are independent of temperature and the density of the liquid and solid phase are assumed to be identical;

(5) Heat loss to the environment due to convection and surface radiation is neglected. These effects can be very easily included in the thermal model. However, an early work in laser cutting [9] indicated that the heat loss due to convection and radiation is negligible for all cases including a sonic assist jet blowing across the surface.

The laser–material interaction can be divided into three stages. During the first stage, the temperature of the solid is below the melting point and therefore no melting or vaporization occurs. The solid absorbs the thermal energy and the temperature of the solid is increased with increase of time. After the highest temperature of the solid, which is located at the center of the laser beam, reaches the melting point of the target material, the irradiation of laser beam will result in melting of the target material and the process enters its second stage. At the second stage, the surface temperature of the liquid is below the saturation temperature and the vaporization required by thermodynamic equilibrium is negligible. When the highest liquid surface temperature reaches the vaporization temperature of the material, the vaporization occurs at the liquid surface and the third stage starts. During the third stage, the locations of both solid–liquid and liquid–vapor interfaces are unknown and need to be determined. From the above explanation, it is clear that the different locations under the irradiation of the laser beam can be at different stages at the same time since the intensity of the laser beam is varied with the radial locations.

Assuming vaporization has started and the liquid–vapor interface is formed, the geometric shape of the liquid–vapor interface and solid–liquid interface are, respectively, expressed as:

$$z = s_1(r, t) \quad (2)$$

$$z = s_2(r, t). \quad (3)$$

Equations (2) and (3) can also be written as

$$f_1(z, r, t) = z - s_1(r, t) = 0 \quad (2a)$$

$$f_2(z, r, t) = z - s_2(r, t) = 0. \quad (3a)$$

The temperatures at the two interfaces satisfy the following conditions

$$T = T_{\mathrm{sat}}, \quad z = s_1(r, t) \quad (4)$$

$$T = T_{\mathrm{m}}, \quad z = s_2(r, t). \quad (5)$$

The energy balance at the liquid–vapor interface can be expressed as

$$\alpha_{\mathrm{abs}} I(r, t) = \rho h_{\mathrm{lv}} \frac{\partial s_1}{\partial t} - k_{\mathrm{l}} \frac{\partial T}{\partial n_1} |\nabla f_1|. \quad (6)$$

It should be noted that equation (6) is not convenient in the determination of the location of the interface. The temperature gradient at the interface, $\partial T/\partial n_1$, can be expressed as [13]:

$$\frac{\partial T}{\partial n_1} = \frac{1}{|\nabla f_1|} \frac{\partial T}{\partial z} \left[1 + \left(\frac{\partial s_1}{\partial r} \right)^2 \right] \quad (7)$$

where

$$|\nabla f_1| = \sqrt{\left(\frac{\partial f_1}{\partial z} \right)^2 + \left(\frac{\partial f_1}{\partial r} \right)^2} = \sqrt{1 + \left(\frac{\partial s_1}{\partial r} \right)^2}. \quad (8)$$

Substituting equations (7) and (8) into equation (6), the energy balance at the liquid–vapor interface becomes

$$\rho h_{\mathrm{lv}} \frac{\partial s_1}{\partial t} = \alpha_{\mathrm{abs}} I(r, t) + k_{\mathrm{l}} \frac{\partial T_{\mathrm{l}}}{\partial z} \left[1 + \left(\frac{\partial s_1}{\partial r} \right)^2 \right], \quad z = s_1(r, t). \quad (9)$$

The intensity of the laser beam is considered as Gaussian spatially and a step function of time. For a single pulse, the intensity is not a function of time during the pulse-on time, i.e.

$$I(r, t) = I_0 \exp\left(-\frac{r^2}{R^2} \right) = \frac{P_{\max}}{\pi R^2} \exp\left(-\frac{r^2}{R^2} \right) \quad t < t_{\mathrm{p}} \quad (10)$$

here I_0 is the peak intensity at the center of the laser beam and R is defined as radius that laser intensity is $1/e$ of the peak intensity. $P_{\max}$ is peak power of the laser beam.

In reference to assumption number 3, the derivative of temperature along the z-direction is expressed as

$$\frac{\partial T_{\mathrm{l}}}{\partial z} = \frac{T_{\mathrm{m}} - T_{\mathrm{sat}}}{s_2 - s_1}, \quad s_1(r, t) \leqslant z \leqslant s_2(r, t). \quad (11)$$

When temperature gradient in equation (9) is substituted by equation (11), the latent heat of vaporization, h_{lv}, needs to be replaced by h'_{lv} to account for the sensible heat absorbed by the liquid layer to bring its average temperature to the average value of melting point and saturation temperature. Substituting equations (1), (10) and (11) and into equation (9), one obtains

$$\frac{\partial s_1}{\partial t} = \frac{\alpha_{\mathrm{abs}} I_0 \, \mathrm{e}^{-\frac{r^2}{R^2}} - k_{\mathrm{l}} \dfrac{T_{\mathrm{sat}} - T_{\mathrm{m}}}{s_2 - s_1} \left[1 + \left(\dfrac{\partial s_1}{\partial r} \right)^2 \right]}{\rho \left[h_{\mathrm{lv}} + \dfrac{1}{2} c_{\mathrm{pl}}(T_{\mathrm{sat}} - T_{\mathrm{m}}) \right]}, \quad z = s_1(r, t). \quad (12)$$

Similarly, the energy balance at the solid–liquid interface can be expressed as [13]

$$\rho h_{\mathrm{sl}} \frac{\partial s_2}{\partial t} = \left[k_{\mathrm{s}} \frac{\partial T_{\mathrm{s}}}{\partial z} - k_{\mathrm{l}} \frac{\partial T_{\mathrm{l}}}{\partial z} \right] \left[1 + \left(\frac{\partial s_2}{\partial r} \right)^2 \right]$$

i.e.

$$\frac{\partial s_2}{\partial t}=\frac{\left[k_s\frac{\partial T_s}{\partial z}+k_l\frac{T_{sat}-T_m}{s_2-s_1}\right]\left[1+\left(\frac{\partial s_2}{\partial r}\right)^2\right]}{\rho h_{sl}},\quad z=s_2(r,t). \tag{13}$$

Kar and Mazumder [7] and Kar et al. [8] assumed that the vaporization temperature, T_{sat}, equals to saturation temperature of liquid metal at ambient pressure. In fact, vaporization occurs after melting creates a back pressure and therefore the vaporization occurs at a higher temperature, i.e., the saturation temperature corresponding to the back pressure. The effect of back pressure on the saturation temperature can be considered through the Clausius/Clapeyron equation. Bellantone and Ganesh [14] and Ganesh et al. [1] derived an equation of saturation temperature by a gas dynamic model, i.e.

$$\frac{\gamma+1}{\gamma h_{lv}}\sqrt{\gamma R_g T_{sat}}\left(I_{abs}+k_l\frac{\partial T_l}{\partial n_l}\right)=p_0\exp\left[\frac{h_{lv}}{R_g}\left(\frac{1}{T_{sat,0}}-\frac{1}{T_{sat}}\right)\right] \tag{14}$$

where, I_{abs} is the rate of energy absorption along normal direction of the liquid–vapor interface, n_l. The terms in the parentheses on the left hand side can be obtained by energy balance in the normal direction of liquid–vapor interface, n_l, which can be obtained from the energy balance in z-direction.

By rearranging equation (6), one can obtain:

$$I_{abs}+k_l\frac{\partial T}{\partial n}=\frac{\alpha_{abs}I(r,t)}{|\nabla f_l|}+k_l\frac{\partial T}{\partial n}=\frac{\rho h_{lv}}{|\nabla f_l|}\frac{\partial s_l}{\partial t}. \tag{6a}$$

Substituting equation (8) into equation (6a) yields

$$I_{abs}+k_l\frac{\partial T_l}{\partial n_l}=\frac{\rho h_{lv}}{\sqrt{1+\left(\frac{\partial s_l}{\partial r}\right)^2}}\frac{\partial s_l}{\partial t}. \tag{6b}$$

Substituting equation (6b) into equation (9), one can obtain

$$\frac{\gamma+1}{\gamma}\sqrt{\gamma R_g T_{sat}}\rho\frac{\partial s_l}{\partial t}=p_0\exp\left[\frac{h_{lv}}{R_g}\left(\frac{1}{T_{sat,0}}-\frac{1}{T_{sat}}\right)\right]\sqrt{1+\left(\frac{\partial s_l}{\partial r}\right)^2}. \tag{15}$$

By using the dimensionless variables defined in the Nomenclature, equations (12), (13) and (15) become

$$\frac{\partial S_1}{\partial\tau}=\frac{N_i\,e^{-\eta^2}-\frac{Ste\,\theta_{sat}}{S_2-S_1}\left[1+\left(\frac{\partial S_1}{\partial\eta}\right)^2\right]}{\left(1+\frac{1}{2}Ste\,\theta_{sat}\right)},\quad Z=S_1(\eta,\tau) \tag{16}$$

$$\frac{\partial S_2}{\partial\tau}=\left[\frac{R_h\,Ste\,\theta_{sat}}{S_2-S_1}+N_\alpha Sc\frac{\partial\theta_s}{\partial Z}\right]\left[1+\left(\frac{\partial S_2}{\partial\eta}\right)^2\right],\quad Z=S_2(\eta,\tau) \tag{17}$$

$$\sqrt{\theta_{sat}(1-\theta_m)+\theta_m}\frac{\partial S_1}{\partial\tau}=N_{p0}\times\exp\left[H_{lv}\left(1-\frac{1}{\theta_{sat}(1-\theta_m)+\theta_m}\right)\right]\sqrt{1+\left(\frac{\partial S_1}{\partial\eta}\right)^2}. \tag{18}$$

The above dimensionless equations are not a closed system because the temperature gradient in the solid is still unknown at this point.

3. Heat conduction in the solid phase

In order to find a simple approximate solution of conduction heat loss, it is assumed that the conduction takes place only in the local surface normal, i.e. the conduction in the solid is assumed to be locally 1-D. The conduction equation in the solid phase will be given at a transformed coordinate system, n_2, which represents non-dimensional distance from a solid–liquid interface location pointing into the solid along the local surface normal. The coordinate system, n_2, rides at the solid–liquid interface. The entire solid moves through the origin of n_2 with the solid–liquid interface moving velocity, V_n, into negative n_2-direction. The heat conduction equation in the solid phase is expressed as [10]

$$\frac{\partial(dA\theta_s)}{\partial\tau}-V_n\frac{\partial(dA\theta_s)}{\partial n_2}=N_\alpha\frac{\partial}{\partial n_2}\left(dA\frac{\partial\theta_s}{\partial n_2}\right) \tag{19}$$

where $dA(n)$ is a non-dimensional local conduction cross section, which is a function of n_2 and allows one to estimate the effects of curvature on the conduction heat loss [10]. For the laser drilling problem, $dA(n)$ can be expressed as follows

$$dA(n)\doteq dA(0)(1+an_2) \tag{20}$$

where

$$a=-\frac{\partial^2 S_2}{\partial\eta^2}\left[1+\left(\frac{\partial S_2}{\partial\eta}\right)^2\right]^{-3/2}. \tag{21}$$

Integrating equation (19) with respect to n_2 in the interval of $(0,\delta)$, where δ is the thickness of thermal penetration depth along the n_2-direction, and consider the following conditions from the definition of thermal penetration depth [13]

$$\theta_s(n_2)|_{n_2=\delta}=0 \tag{22}$$

$$\left.\frac{\partial\theta_s}{\partial n_2}\right|_{n_2=\delta}=0 \tag{23}$$

one can obtain the integral equation of the conduction problem

$$\frac{\mathrm{d}}{\mathrm{d}\tau}\int_0^{\delta}(1+an_2)\theta_s\,\mathrm{d}n_2+V_n\theta_{s0}=-N_\alpha\left.\frac{\partial\theta_s}{\partial n_2}\right|_{n_2=0}. \tag{24}$$

The temperature distribution in the penetration depth is assumed to be a second-order polynomial function and the constants in the polynomial function can be determined by equations (22) and (23). The final form of the temperature distribution is

$$\theta_s=\theta_{s0}\left(1-\frac{n_2}{\delta}\right)^2,\quad n_2\leqslant\delta, \tag{25}$$

Substituting equation (25) into equation (24), one can obtain a differential equation of the thermal penetration depth as follows

$$\frac{\mathrm{d}}{\mathrm{d}\tau}\left[\theta_{s0}\delta\left(1+\frac{1}{4}a\delta\right)\right]+3V_n\theta_{s0}=\frac{6N_\alpha\theta_{s0}}{\delta}. \tag{26}$$

It should be noted that both V_n and $\partial S_2/\partial\tau$ are solid–liquid interface moving velocities. The difference between these two velocities is that the former is velocity along n_2-direction but the latter is the velocity along Z-direction. These two velocities have the following relationship [13]

$$V_n=\frac{\partial S_2}{\partial\tau}\Big/\sqrt{1+\left(\frac{\partial S_2}{\partial\eta}\right)^2}. \tag{27}$$

Substituting equation (27) into equation (26), the differential equation of δ becomes

$$\frac{\mathrm{d}}{\mathrm{d}\tau}\left[\theta_{s0}\delta\left(1+\frac{1}{4}a\delta\right)\right]+3\theta_{s0}\frac{\partial S_2}{\partial\tau}\Big/\sqrt{1+\left(\frac{\partial S_2}{\partial\eta}\right)^2}=\frac{6N_\alpha\theta_{s0}}{\delta}. \tag{28}$$

The goal of the solution of the heat conduction is to provide the temperature gradient in the solid at the solid–liquid interface so that the effect of conduction heat loss can be considered. During the second and third stages, the solid–liquid interface temperature is kept at the melting point of the material, i.e.

$\theta_{s0}=1.$

At second and third stages, equation (28) is simplified as

$$\frac{\mathrm{d}}{\mathrm{d}\tau}\left[\delta\left(1+\frac{1}{4}a\delta\right)\right]+3\frac{\partial S_2}{\partial\tau}\Big/\sqrt{1+\left(\frac{\partial S_2}{\partial\eta}\right)^2}=\frac{6N_\alpha}{\delta}. \tag{29}$$

The temperature gradient in the solid at the solid–liquid interface can be obtained from equation (25)

$$\left.\frac{\partial\theta_s}{\partial n_2}\right|_{n_2=0}=-\frac{2}{\delta}. \tag{30}$$

The energy balance at the solid–liquid interface, equation (17), requires the derivative of the temperature in the solid phase, θ_s, with respect to Z. Therefore, the following relationship [13] is needed.

$$\frac{\partial\theta_s}{\partial Z}=\frac{\partial\theta_s}{\partial\eta}\Big/\sqrt{1+\left(\frac{\partial S_2}{\partial\eta}\right)^2}. \tag{31}$$

Substituting equations (30) and (31) into equation (17), one obtains

$$\frac{\partial S_2}{\partial\tau}=\frac{R_h\,Ste\,\theta_{sat}}{S_2-S_1}\left[1+\left(\frac{\partial S_2}{\partial\eta}\right)^2\right]-\frac{2N_\alpha Sc}{\delta}\sqrt{1+\left(1+\left(\frac{\partial S_2}{\partial\eta}\right)^2\right)},\quad Z=S_2(\eta,\tau). \tag{32}$$

4. Solving procedure

4.1. Duration of preheating (*first stage*)

During the first stage, the solid–liquid interface moving velocity is zero since melting does not occur. In this case, equation (28) can be simplified as

$$\frac{\mathrm{d}}{\mathrm{d}\tau}(\theta_{s0}\delta)=\frac{6N_\alpha\theta_{s0}}{\delta}. \tag{33}$$

An additional equation for θ_{s0} is required in order to solve equation (33). This additional equation is obtained by the energy balance at the solid surface before start of melting. Before start of melting, the solid surface is a flat surface and therefore, the coordinate system of n_2 and Z are identical.

The energy balance at the solid surface is expressed as

$$-k_s\frac{\partial T_s}{\partial z}=\alpha_{abs}I_0\exp\left(-\frac{r^2}{R^2}\right). \tag{34}$$

Equation (34) can be nondimensionalized by using the dimensionless variables defined in the Nomenclature, i.e.

$$\left.\frac{\partial\theta_s}{\partial Z}\right|_{Z=0}=-\frac{R_hN_i}{N_\alpha Sc}\mathrm{e}^{-\eta^2}. \tag{35}$$

Substituting equation (25) into equation (35) and noticing the fact of $n_2=Z$ at first stage, one may obtain

$$\theta_{s0}=\frac{R_hN_i\delta}{2N_\alpha Sc}\mathrm{e}^{-\eta^2}. \tag{36}$$

Substituting equation (36) into equation (33), an ordinary differential equation is obtained

$$\frac{\mathrm{d}\delta^2}{\mathrm{d}\tau}=6N_\alpha. \tag{37}$$

Integrating equation (37) and considering the initial condition of

$$\delta=0,\quad \tau=0 \tag{38}$$

an expression of thermal penetration depth, δ, for the first stage is obtained

$$\delta=\sqrt{6N_\alpha\tau}. \tag{39}$$

It is noted that the thermal penetration depth is not a

function of radial coordinate, η. The solid surface temperature is obtained by substituting equation (39) into equation (36), i.e.

$$\theta_{s0} = \frac{R_h N_i \sqrt{6N_\alpha \tau}}{2N_\alpha Sc} e^{-\eta^2}. \quad (40)$$

During this stage, the dimensionless solid surface temperature, θ_{s0}, should always be less than one. The melting starts when θ_{s0} reaches to one. Thus, the preheating time, τ_m, can be obtained by applying $\theta_{s0} = 1$ in equation (40) and solving for τ_m, i.e.

$$\tau_m(\eta) = \frac{1}{6N_\alpha}\left(\frac{2N_\alpha Sc}{R_h N_i} e^{\eta^2}\right)^2. \quad (41)$$

It can be seen that the preheating time is shortest at the center of the laser beam and the melting starts at the center first.

4.2. Melting before the start of vaporization (second stage)

At the second stage, the liquid surface temperature is below the saturation temperature and therefore the liquid–vapor interface velocity is zero. The dimensionless liquid surface temperature, θ_{l0}, which is defined as

$$\theta_{l0} = \frac{T_{l0} - T_m}{T_{sat,0} - T_m} \quad (42)$$

can be obtained by energy balance at the liquid surface, i.e.

$$\theta_{l0} = \frac{N_i S_2 e^{-2\eta^2}}{Ste}. \quad (43)$$

The energy balance at the solid–liquid interface during this stage can be obtained by replacing θ_{sat} in equation (32) by θ_{l0} because the liquid surface temperature is actually θ_{l0}. It is also noted that the location of liquid–vapor interface during this stage is $S_1 = 0$. Therefore, the energy balance at the solid–liquid interface during this stage is expressed as

$$\frac{\partial S_2}{\partial \tau} = \frac{R_h\, Ste\, \theta_{l0}}{S_2}\left[1 + \left(\frac{\partial S_2}{\partial \eta}\right)^2\right] - \frac{2N_\alpha Sc}{\delta}\sqrt{1 + \left(\frac{\partial S_2}{\partial \eta}\right)^2}, \quad Z = S_2(\eta, \tau). \quad (44)$$

Substituting equation (43) into equation (44), the energy balance at the solid–liquid interface becomes

$$\frac{\partial S_2}{\partial \tau} = R_h N_i e^{-\eta^2}\left[1 + \left(\frac{\partial S_2}{\partial \eta}\right)^2\right] - \frac{2N_\alpha Sc}{\delta}\sqrt{1 + \left(\frac{\partial S_2}{\partial \eta}\right)^2}, \quad Z = S_2(\eta, \tau). \quad (45)$$

Vaporization will not occur if the surface temperature of the liquid, T_{l0}, is below the vaporization temperature, $T_{sat,0}$, i.e., $\theta_{l0} \geqslant 0$. Therefore, the critical value of S_2, below which vaporization will not occur, can be obtained by applying this condition to equation (45).

$$S_{2cr}(\eta) = \frac{Ste}{N_i} e^{\eta^2}. \quad (46)$$

The critical value, S_{2cr} obtained from equation (46) is a criterion to determine if vaporization occurs. It can be seen that the vaporization starts from the center of the laser beam. The solution of the second stage requires solving equations (45) and (29) simultaneously.

4.3. Vaporization and melting in the third stage

The solution in the third stage is most complicated because vaporization, melting and conduction in the solid have to be solved simultaneously. These partial differential equations can be discretalized by an implicit finite difference scheme [15] and solved by an iteration method.

5. Results and discussion

The absorptivity of target materials is a very important property for thermal modeling of the material processing. It depends on the wavelength of the laser beam and the target material. It is usually higher for a laser beam with shorter wave length (such as Nd : YAG) and lower for a laser beam with longer wavelength (such as CO_2). Its value is usually very low for most metals at room temperature, but it increases with increase of the target material temperature [16]. While no general expression can be applied, Ganesh et al. [1, 12] assumed that the surface temperature of the target materials is high enough so that the reflectively can be neglected and therefore the absorptivity was set to unity in refs [1, 12]. It is rather high because the absorptivity can become unity only for deep holes with plasma (keyhole). Kar et al. [8] gave a very detailed review of the absorptivity of metal under irradiation of laser beam in the existing literature. They recommended that the appropriate value of absorptivity for laser drilling would be 0.85. The reason for such a high absorptivity is that the laser beam can propagate through the liquid film present in the cavity to cause volumetric heat generation and result in a high value of effective absorptivity. It should be noted that the absorptivity does not appear in the dimensionless governing equations and therefore the results of parametric study based on the dimensionless governing equations performed in this paper will not be affected by the value of absorptivity.

The laser drilling on a workpiece made of Hastelloy-X is first simulated and the results are compared with the experimental data in ref. [14]. The thermal properties of the liquid Hastelloy-X are available from ref. [14]. However, the thermal properties of solid phase, which is very important to calculate the conduction heat loss, are not available. This problem can be overcome by using the properties of superalloy [4] which are more or less

closer to that of Hastelloy-X [12]. In order to obtain dimensional results for comparison, the value of absorptivity of the target materials is needed and it will be taken as 0.85 as recommended by Kar et al. [8]. In order to obtain high accuracy numerical results, double precision variables are used in the FORTRAN code. The results in Fig. 2 were obtained by using a grid number of $N = 60$ with a dimensionless time step of $\Delta\tau = 10^{-6}$. Although a larger grid number and smaller dimensionless time step ($N = 90$, $\Delta\tau = 10^{-7}$) were also used to simulate a few cases, no distinguishable differences were found. The average material removal rate in the laser drilling process, which is obtained by the following integration

$$MR = \frac{2\pi\rho}{t_p}\int_0^\infty s_1(r, t_p) r\,dr \tag{47}$$

will be compared with experimental data. It should be noted that the dimensional form of variables are used in equation (47) in order to compare with the experimental data. The comparison of calculated material removal rate, for the cases with and without conduction heat loss, and that of experimental data is shown in Fig. 2. The experimental material removal rate was obtained by scaling micrographs of single shot drilled holes for pulse-on time of 700 μs and radius of 0.254 mm at the Pratt and Whitney drilling facility at North Haven, CT [14]. It can be seen that the predicted materials removal rate with conduction heat loss is slightly lower than that without conduction heat loss but the difference is less than 2%. This suggests that the overall effect of conduction heat loss on the material removal rates is not significant. As can be seen from Fig. 2, the material removal rate predicted by the present model is higher than that of experimental data for most cases. The possible cause of the over prediction may include uncertainty of absorptivity and possible partial laser beam blockage due to plasma, which is not taken into account in the model. Considering these complicated phenomena, the agreement between

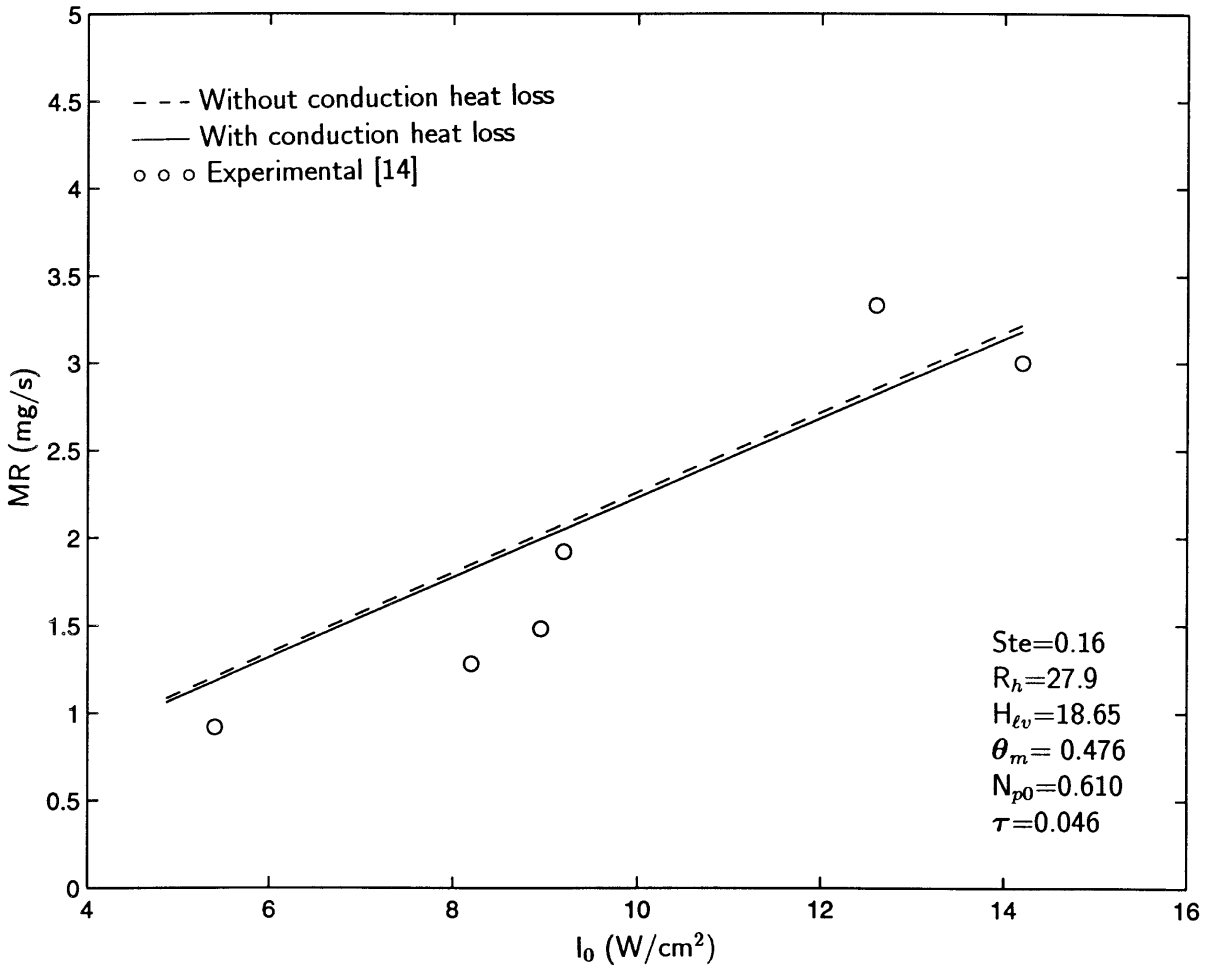

Fig. 2. Comparison of predicted and experimental material removal rate.

calculated results and the experimental data is very good.

Figure 3 shows the effect of subcooling on the liquid–vapor and solid–liquid interfaces. As can be seen, both vaporization and melting velocity is decreased due to the effect of subcooling in the target material. The effect of subcooling on the velocity of vaporization is very small. However, the melting velocity is more affected by the subcooling since the conduction heat loss directly reduces the energy that can be used to melt the target material. Since vaporization is the mechanism of material removal and vaporization is less affected by subcooling, the material removal rate for the case with conduction heat loss only 2% less than that without conduction heat loss (see Fig. 2). It is also noted that the effect of conduction heat loss on the liquid–vapor interface are the same at different locations. However, the conduction heat loss has more significant effect on the solid–liquid interface at the locations far from the center of the laser beam where the laser intensity is weaker. Therefore, existence of subcooling resulted in thinner liquid layer. Figure 4 shows the effect of subcooling on the liquid–vapor and solid–liquid interfaces for different laser properties. The total laser energy absorbed by the target materials are the same as Fig. 3 because the laser intensity of the case in Fig. 4 is half that in Fig. 3 but the pulse-on time of the case in Fig. 4 is two times of that in Fig. 3. It can be seen that the effect of subcooling on both liquid–vapor and solid–liquid interfaces is more significant for the case of low intensity and longer pulse-on time. Another phenomenon that we can observe from Figs 3 and 4 is that the laser intensity and pulse-on time have very little effect on the liquid–vapor interface but their effect on the solid–liquid interface turns out to be more significant. Therefore, lower laser intensity and longer pulse-on time would result in thicker liquid layer.

It will be useful to analyze the effect of subcooling on the thickness of the liquid layer because this liquid layer will be resolidified to form a recast layer after the drilling

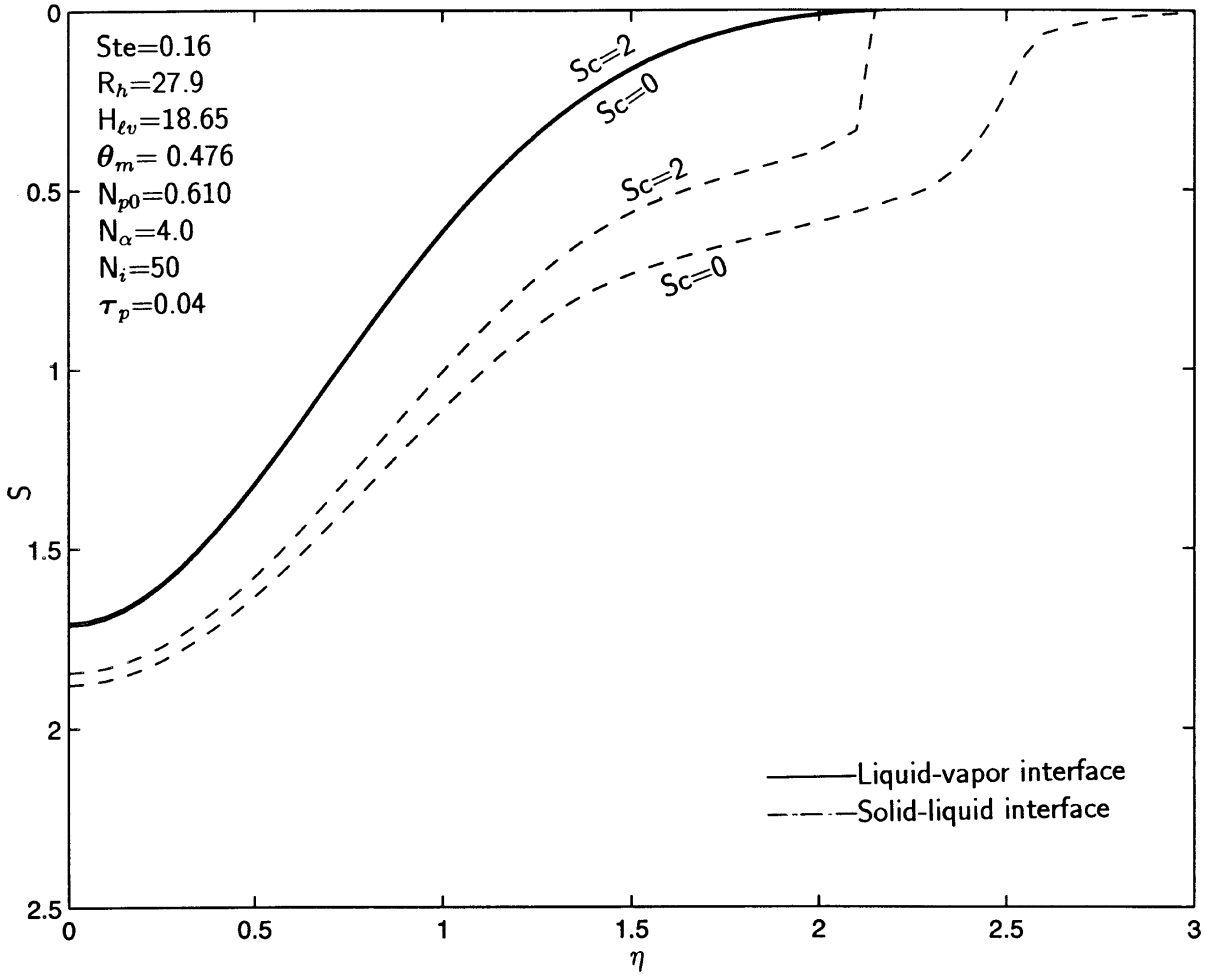

Fig. 3. Effect of conduction heat loss on the liquid–vapor and solid–liquid interfaces ($N_i = 60$, $\tau_p = 0.04$).

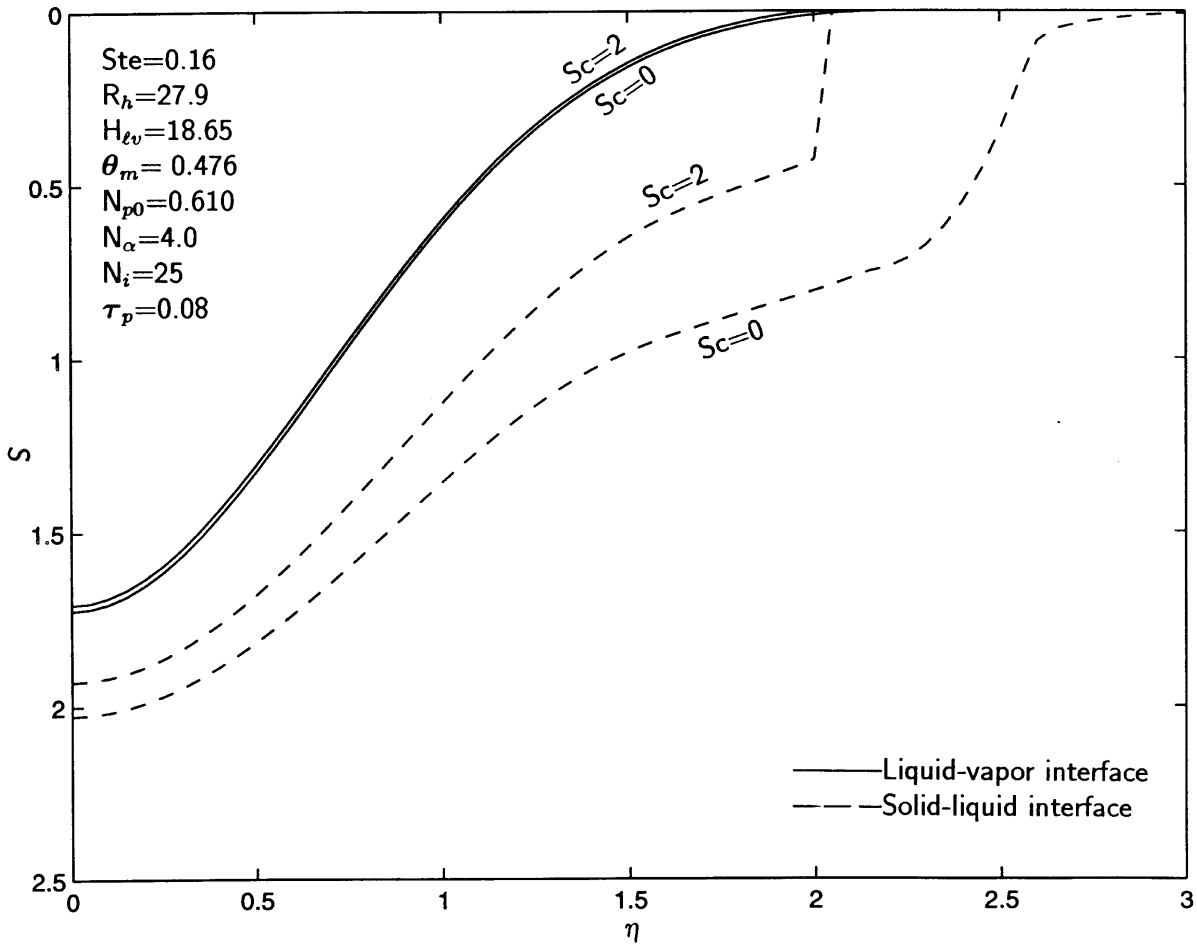

Fig. 4. Effect of conduction heat loss on the liquid–vapor and solid–liquid interfaces ($N_i = 30$, $\tau_p = 0.08$).

process is completed [7]. It can be seen that the liquid layer is thinner if subcooling exists in the solid phase or the laser intensity is higher and pulse-on time is longer. Since the thermal and mechanical properties of the recast layer may be different from those of the original target materials, the thinner liquid layer is always desirable. The higher laser intensity, shorter pulse-on time and the existence of subcooling will be helpful to reduce the recast layer thickness.

The heat generated by the laser beam is divided into three parts: conduction heat loss, latent heat of solid–liquid phase change and liquid–vapor phase change. If the fractions of heat goes to these three parts are, respectively, represented by F_c, F_{sl} and F_{lv}, the following condition has to be satisfied.

$$F_c(\eta,\tau)+F_{sl}(\eta,\tau)+F_{lv}(\eta,\tau)=1. \quad (48)$$

It should be pointed out that the fractions of heat goes to three parts, which is determined by analyzing equations (9) and (28), are the functions of both location and time. Figure 5 shows the variations of the fractions of heat goes to three different parts with time at the center of the laser beam ($\eta = 0$) for the case represented by Fig. 3. As can be seen, all of the heat generated by the laser beam at the first stage goes to the conduction heat loss since no vaporization and melting occur in this stage. During the second stage, which is a very short period of time as appears in Fig. 5, most of the heat generated by the laser beam is used to supply the latent heat of melting and only a small amount of heat is lost by conduction in the solid. At the third stage, the heat used to vaporize the melted liquid significantly increases with time and the heat used to melt the solid significantly decreases with time. The heat lost through conduction to the solid is a constant at the third stage. The fractions of three parts at the center of the laser beam will become constant when the time is relatively large. It should be pointed out that the time axis in Fig. 3 is significantly exaggerated and

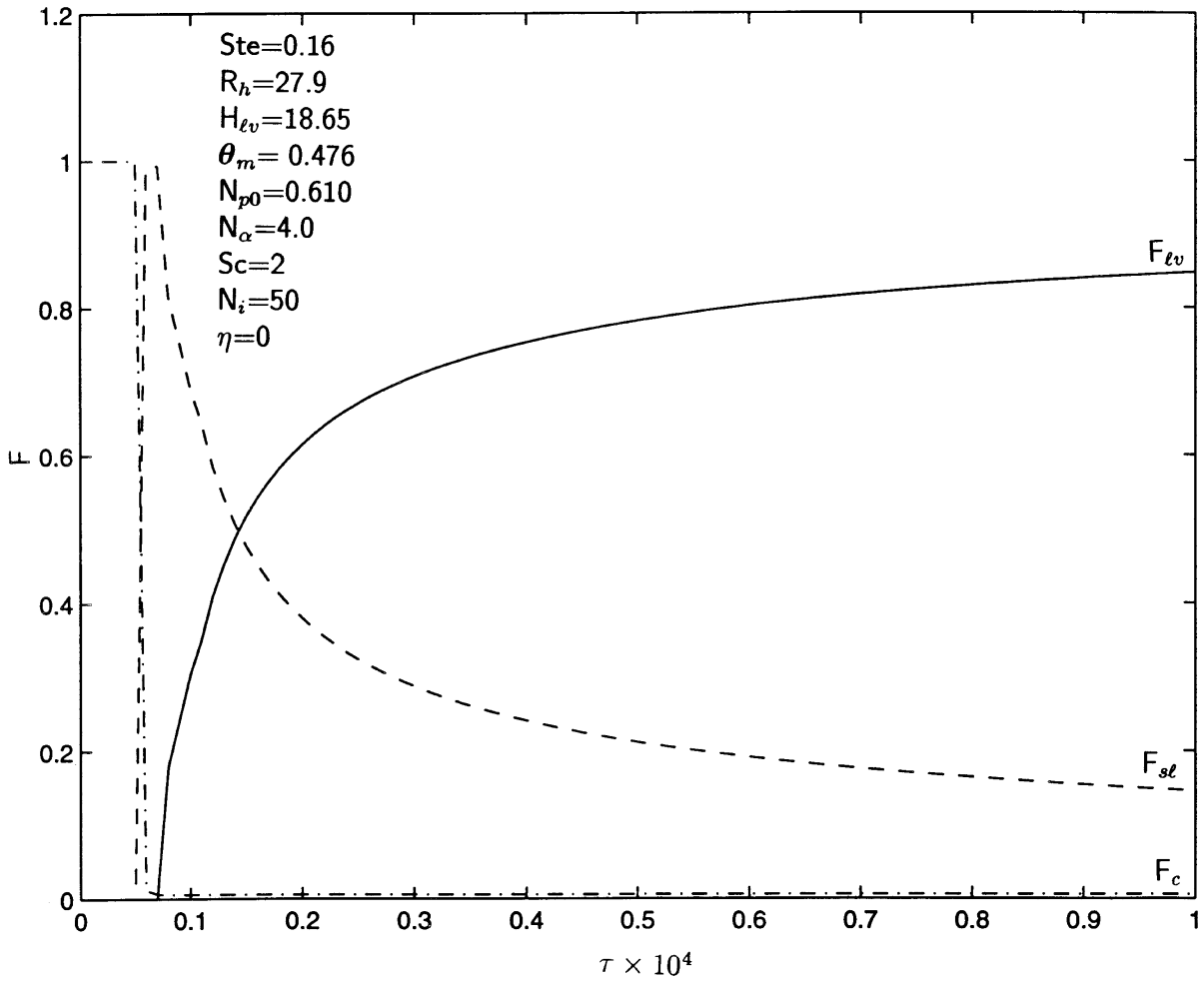

Fig. 5. Fractions of heat used to conduction heat loss, melting and vaporization at the center of the laser beam ($N_i = 60$, $\tau_p = 0.04$).

only reflect the very beginning of the drilling process. In fact, the variation of the heat goes to the three parts is very fast and therefore the fractions of the heat go to the three parts are constants for most periods of the drilling process other than the very beginning period. The fractions of heat that goes to three parts for the case represented by Fig. 4 is shown in Fig. 6. Basically, the variation of the fractions is similar to that in Fig. 5 except the times of first and second stages are longer and the fraction of conduction loss is higher than that in Fig. 6.

Figure 7 shows the fractions of the heat lost through conduction, melting and vaporization with different locations at a fixed time $\tau = 0.04$ for the case represented by Fig. 3. As can be seen, the fraction of conduction heat loss at the center of the laser beam is very small (0.5%) and increases with increase of η since the laser intensity decreases with increase of η. At edge of the laser beam, where no vaporization and melting occur due to low laser intensity, the conduction heat loss becomes 100%. The fraction of heat used to supply the latent heat of melting is about 3% at the center of the laser beam and increase with increase of η. At $\eta = 2.1$, F_{sl} reaches 35% and then drop to zero since melting does not occur for larger η. The fraction of heat used to supply the latent heat of vaporization are maximum at the center of the laser beam, 96%, and decreases all the way to 0% at the edge of the laser beam. Although the fraction of heat used to supply latent heat of melting and lost through conduction becomes very large at the locations far from the center of the laser beam, it has very little contribution on the overall heat goes to latent heat of melting and conduction loss. The overall conduction heat loss is very small for this case. Figure 8 shows the fractions of the three parts with different locations at a fixed time $\tau = 0.08$ for the

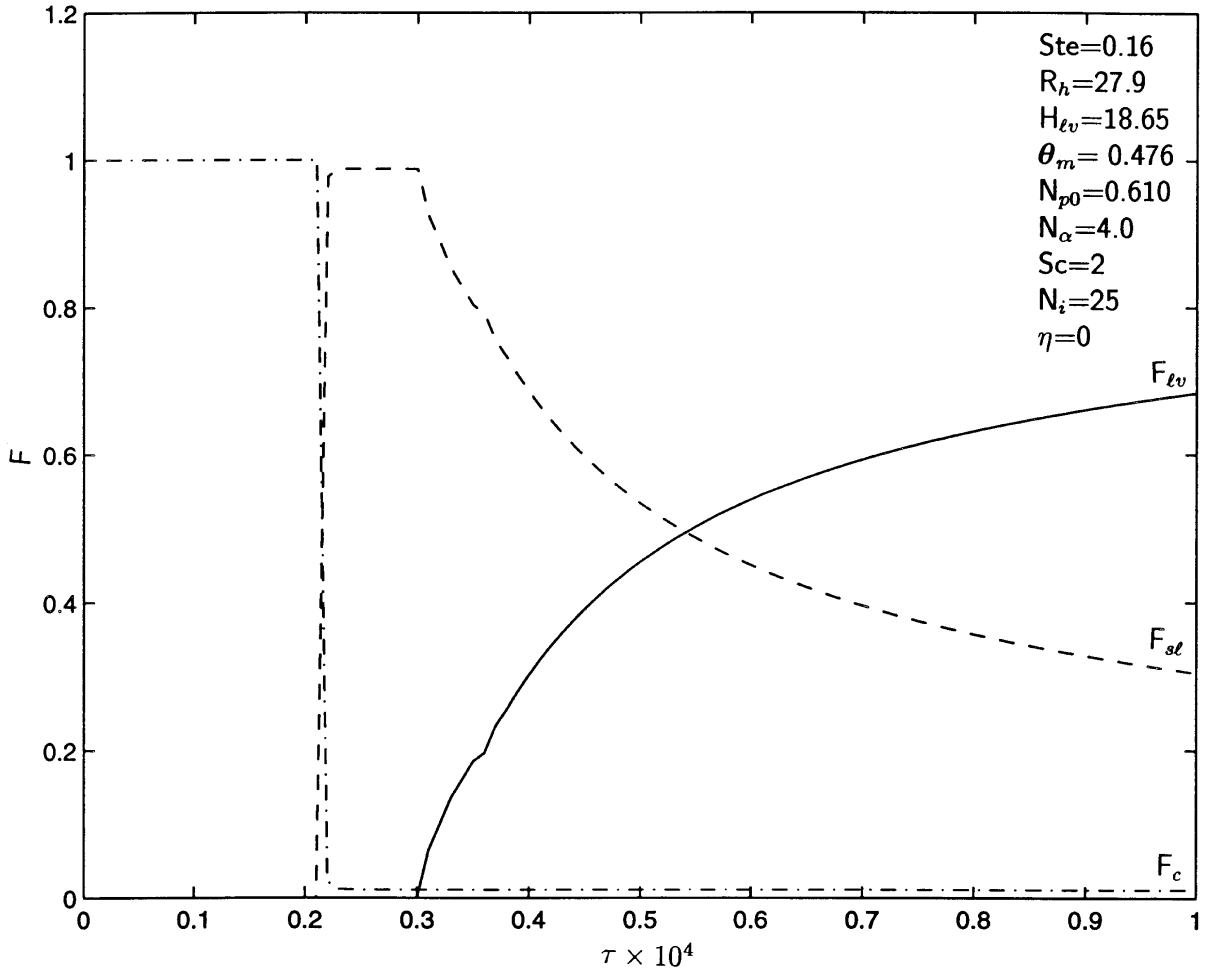

Fig. 6. Fractions of heat used to conduction heat loss, melting and vaporization at the center of the laser beam ($N_i = 30$, $\tau_p = 0.08$).

case represented by Fig. 4. It can be seen that the fraction of heat lost through conduction, which is 1% at the center, is larger than that of the case represented by Fig. 3. Therefore, lower laser intensity and longer pulse result in larger conduction heat loss.

Figure 9 shows the effect of the dimensionless laser intensity on the locations of the solid–liquid and liquid–vapor interfaces at the center of the laser beam. The effects of subcooling on the velocities of liquid–vapor interface are almost the same for different laser intensity. On the other side, the effect of subcooling on the velocity of solid–liquid interface is slightly significant for lower laser intensity. This is due to the fact that the amount of heat which is required to bring the temperature of solid to its melting point is approximately the same for different laser intensity. Therefore, the effect of subcooling on the laser drilling process is more significant for the case using lower laser intensity and longer pulse-on time. Regardless if the subcooling exists in the solid, the thickness of the liquid layer at the center of the laser beam is significantly decreased with increase of laser intensity especially for lower laser intensity. For lower laser intensity, the liquid layer thickness at the center of the laser beam is significantly thinner if subcooling exists in the solid. However, liquid layer thickness is almost not affected by both laser intensity and subcooling parameter if the laser intensity is very high.

6. Conclusion

A thermal model of the melting and vaporization phenomena in the laser drilling process has been developed by energy balance analysis at the solid–liquid and liquid–vapor interfaces. The dependence of saturation temperature on the back pressure was accounted for by the Clausius/Clapeyron equation. The conduction heat loss to the workpiece is also included in the model

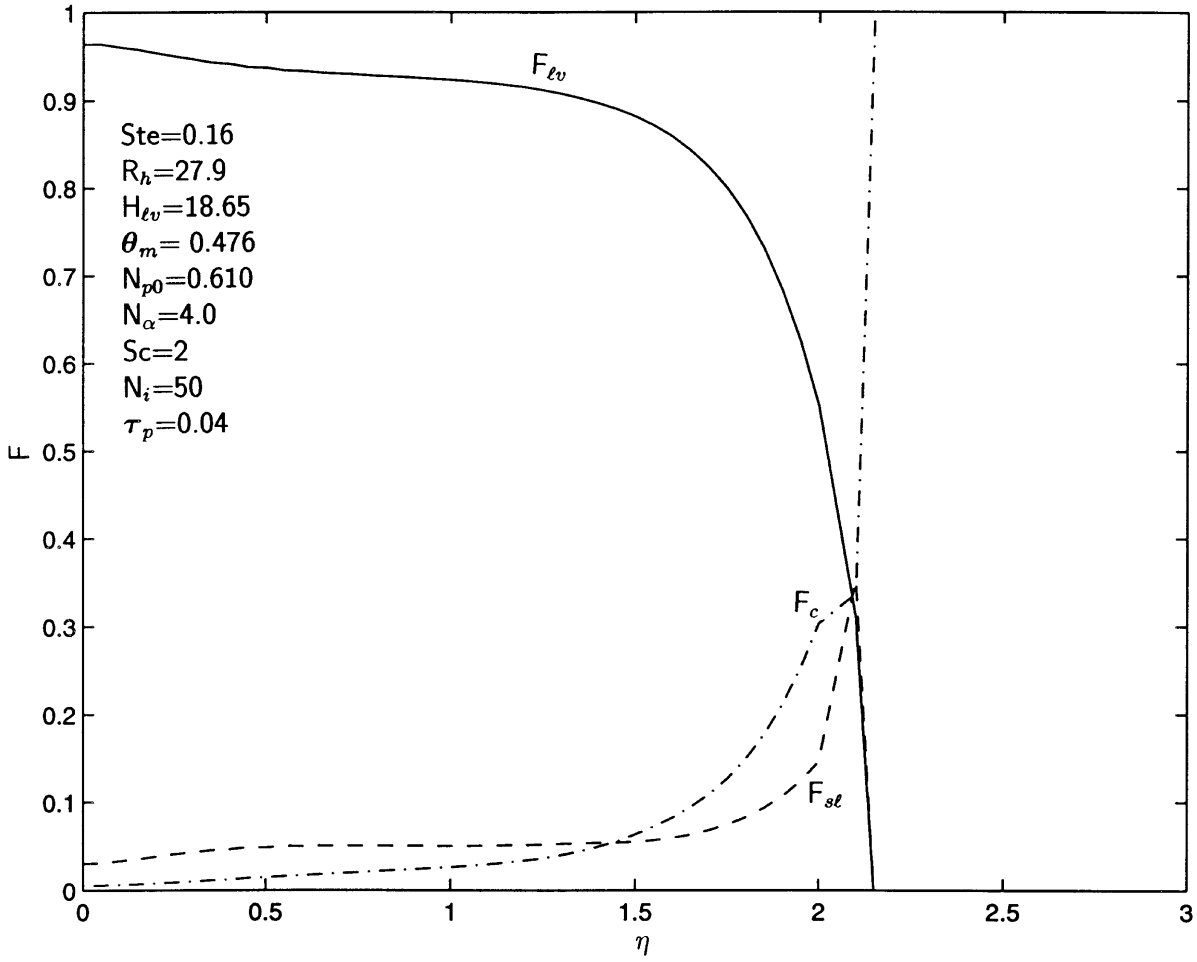

Fig. 7. Fractions of heat used to conduction heat loss, melting and vaporization at different locations ($N_i = 60$, $\tau_p = 0.04$).

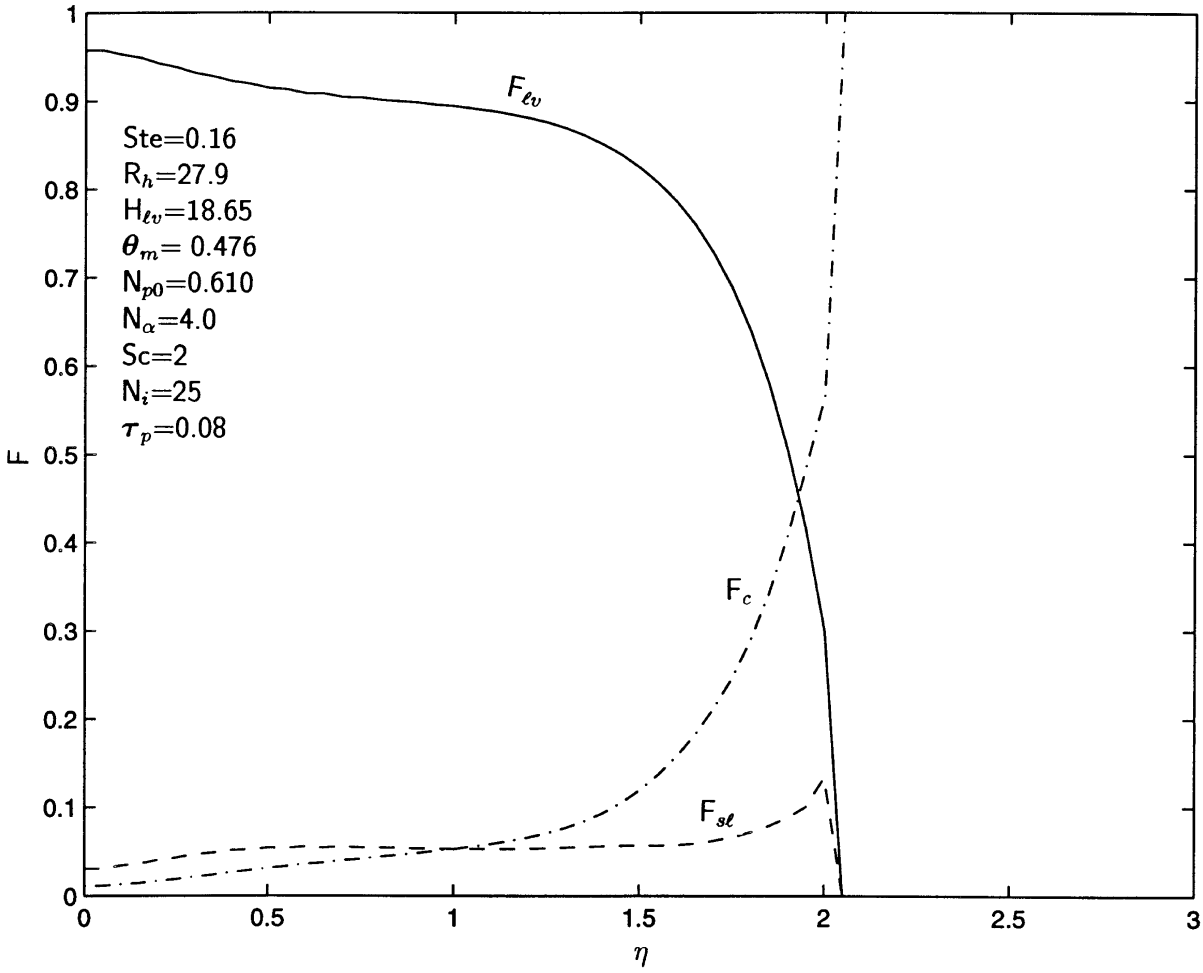

Fig. 8. Fractions of heat used to conduction heat loss, melting and vaporization at different locations ($N_i = 30$, $\tau_p = 0.08$).

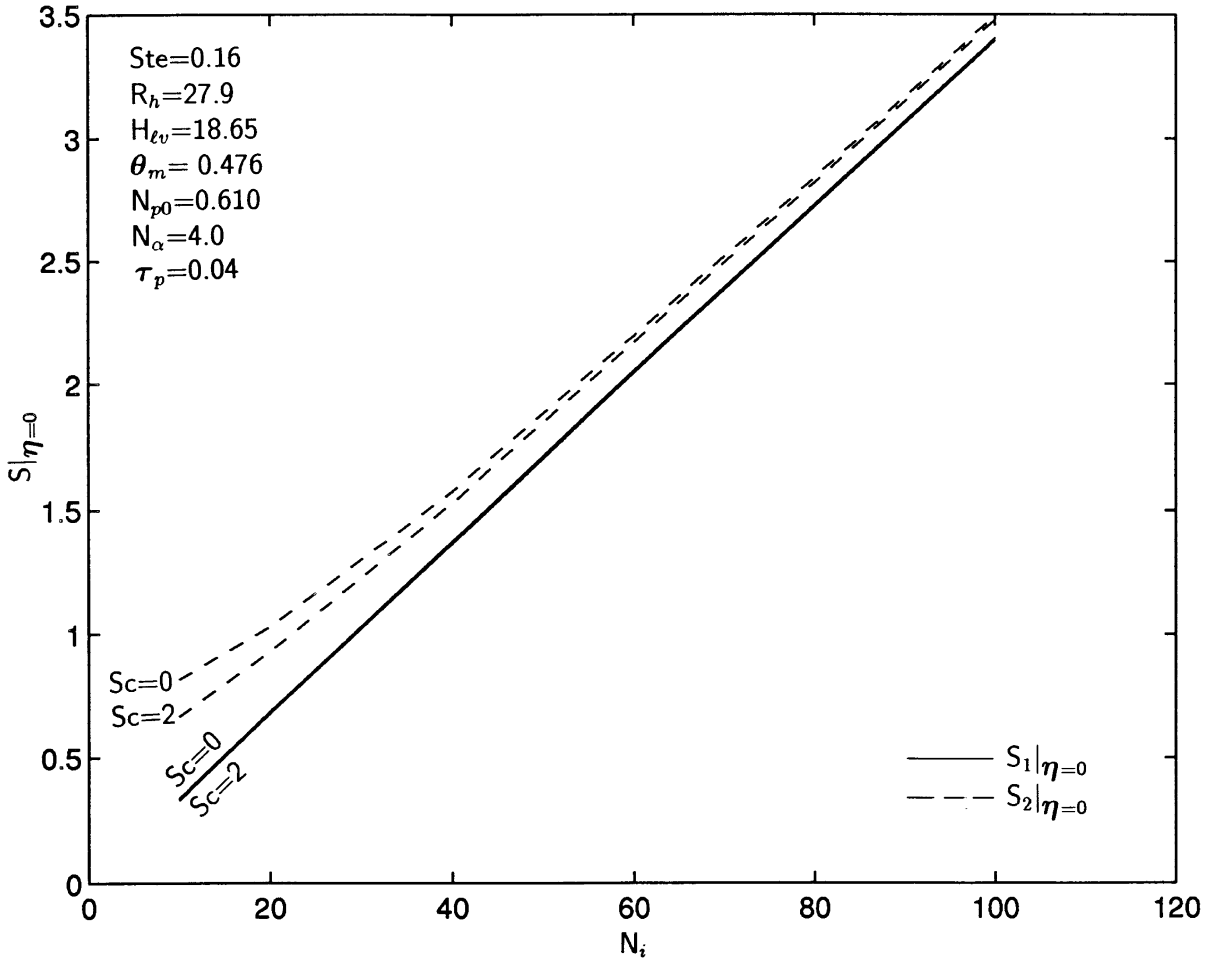

Fig. 9. Effect of the dimensionless laser intensity on the locations of the solid–liquid and liquid–vapor interfaces at the center of the laser beam.

and is solved using an integral approximate method. The predicted material removal rate qualitatively agreed very well with the experiment data. The amount of heat lost through conduction is found to be very small and its effect on the vaporization is not significant. However, the locations of melting front is significantly affected by conduction heat loss especially for lower laser intensity and longer pulse. The existence of subcooling in the solid is helpful in reducing the thickness of recast layer.

References

[1] R.K. Ganesh, A. Faghri, Y. Hahn, A generalized thermal modeling for laser drilling process—I. Mathematical modeling and numerical methodology, Int. J. Heat Mass Transfer 40 (1997) 3351–3360.

[2] U.C. Paek, F.P. Pagliano, Thermal analysis of laser drilling processes, IEEE Journal of Quantum electronics QE-8 (1972) 112–119.

[3] M. Von Allmen, Laser drilling velocity in metals, J. Applied Physics 47 (1976) 5460–5463.

[4] C.L. Chan, J. Mazumder, One-dimensional steady state model for damage by vaporization and liquid expulsion due to laser–material interaction, J. Applied Physics 62 (1987) 4579–4586.

[5] E. Armon, Y. Zvirin, G. Laufer, A. Solan, Metal drilling with a CO_2 laser beam. I. Theory, J. Applied Physics 65 (1989) 4995–5002.

[6] E. Armon, M. Hill, I.J. Spalding, Y. Zvirin, Metal drilling with a CO_2 laser beam. II. Analysis of aluminum drilling experiments, J. Applied Physics 65 (1989) 5003–5006.

[7] A. Kar, J. Mazumder, Two-dimensional model for material damage due to melting and vaporization during laser irradiation, J. Applied Physics 68 (1990) 3884–3891.
[8] A. Kar, T. Rockstroh, J. Mazumder, Two-dimensional model for laser-induced material damage: effect of assist gas and multiple reflections inside the cavity, J. Applied Physics 71 (1992) 2560–2569.
[9] M.F. Modest, H. Abakians, Evaporative cutting of a semi-infinite body with a moving CW laser, ASME J. Heat Transfer 108 (1986) 602–607.
[10] M.F. Modest, Transient model for CW and pulsed laser machining of ablating/decomposing materials—approximate analysis, ASME J. Heat Transfer 118 (1996) 774–780.
[11] M.H. Gordon, M. Touzelbaev, M. Xiao, R.C. Goforth, Numerical simulation of diamond film ablation under irradiation by laser beam, Thermal Processing Materials: Thermo-Mechanics, Controls and Composites, HTD-Vol. 289, Chicago, IL, 1994, pp. 73–77.
[12] R.K. Ganesh, A. Faghri, Y. Hahn, A generalized thermal modeling for laser drilling process—II. Numerical simulation and results, Int. J. Heat Mass Transfer 40(14) (1997) 3361–3373.
[13] M.N. Ozisik, Heat Conduction, Wiley-Interscience, New York, 1980.
[14] R. Bellantone, R.K. Ganesh, Analytical model for laser hold drilling: final report, Contract II, report submitted to Pratt and Whitney Aircraft, East Hartford, CT, 1991.
[15] S.V. Patankar, Numerical Heat Transfer and Fluid Flow, McGraw-Hill, New York, 1980.
[16] M. Von Allmen, Laser-Beam Interactions with Materials, Springer-Verlag, New York, 1986.